Article

# Transformer Meets Convolution: A Bilateral Awareness Network for Semantic Segmentation of Very Fine Resolution Urban Scene Images

Libo Wang 1, †, Rui Li 1, †, Dongzhi Wang 2, \*, Chenxi Duan 3, Teng Wang 2, and Xiaoliang Meng 1

- <sup>1</sup> School of Remote Sensing and Information Engineering, Wuhan University, Wuhan 430079, China; wanglibo@whu.edu.cn (L.W.); lironui@whu.edu.cn (R.L.); xmeng@whu.edu.cn (X.M.)
- <sup>2</sup> Surveying And Mapping Institute Lands And Resource Department Of Guangdong Province, Guangzhou, 510500, China; wangteng43@hotmail.com (T.W.)
- <sup>3</sup> State Key Laboratory of Information Engineering in Surveying, Mapping, and Remote Sensing, Wuhan University, 430079, China; <a href="mailto:chenxiduan@whu.edu.cn">chenxiduan@whu.edu.cn</a> (C.D.)
- \* Correspondence: harwang1984@foxmail.com (D.W.); Tel: 020-38334381
- <sup>†</sup> Equal contribution.

Abstract: Semantic segmentation from very fine resolution (VFR) urban scene images plays a significant role in several application scenarios including autonomous driving, land cover classification, and urban planning, etc. However, the tremendous details contained in the VFR image severely limit the potential of the existing deep learning approaches. More seriously, the considerable variations in scale and appearance of objects further deteriorate the representational capacity of those semantic segmentation methods, leading to the confusion of adjacent objects. Addressing such issues represents a promising research field in the remote sensing community, which paves the way for scene-level landscape pattern analysis and decision making. In this manuscript, we propose a bilateral awareness network (BANet) which contains a dependency path and a texture path to fully capture the long-range relationships and fine-grained details in VFR images. Specifically, the dependency path is conducted based on the ResT, a novel Transformer backbone with memory-efficient multi-head self-attention, while the texture path is built on the stacked convolution operation. Besides, using the linear attention mechanism, a feature aggregation module (FAM) is designed to effectively fuse the dependency features and texture features. Extensive experiments conducted on the three large-scale urban scene image segmentation datasets, i.e., ISPRS Vaihingen dataset, ISPRS Potsdam dataset, and UAVid dataset, demonstrate the effectiveness of our BANet. Specifically, a 64.6% mIoU is achieved on the UAVid dataset.

Keywords: urban scene segmentation; remote sensing; Transformer; attention mechanism

## 1. Introduction

Semantic segmentation of very fine resolution (VFR) urban scene images comprises a hot topic in the remote sensing community [1-6]. It plays a crucial role in various urban applications, such as urban planning [7], vehicle monitoring [8], land cover mapping [9], and change detection [10], as well as building and road extraction [11,12]. The goal of semantic segmentation is to label each pixel with a certain category. Since geo-objects in urban areas are characterized by large within-class and small between-class variance commonly, semantic segmentation of VHR imagery remains a challenging issue [13,14]. For example, urban buildings made of diverse materials show variant spectral signatures, while buildings and roads made of the same material (e.g. cement) exhibit similar textural information.

Due to the advantage in local texture extraction, many researchers have investigated the challenging urban scene segmentation task based on deep convolutional neural networks (DCNNs) [15-17]. Especially, the methods based on fully convolutional neural

network (FCN) [18], which can be trained end-to-end, have achieved great breakthroughs in urban scene labelling [19]. In comparison with the traditional machine learning methods, such as support vector machine (SVM) [20], random forest (RF) [21], and conditional random field (CRF) [22], the FCN-based methods have demonstrated remarkable generalization capability and high efficiency [23,24]. Therefore, numerous specially designed FCN-based networks have been spawned for urban scene segmentation, including UNet and its variants [13,25-27], multi-scale context aggregation networks [28, 57], and multi-level feature fusion networks [5], attention-based networks [29,30], as well as lightweight networks [31]. For example, Sherrah [19] introduced the FCN to semantically label remote sensing images. Kampffmeyer et al. [32] quantified the uncertainty in urban remote sensing images at the pixel level, thereby enhancing the accuracy of relatively small objects (e.g., Cars). Maggiori et al. [33] designed an auxiliary CNN to learn the features fusion schemes. Multi-modal data were further utilized by Audebert et al. [34] further leveraged in their V-FuseNet to enhance the segmentation performance. However, such a multi-modal data fusion scheme will be invalid if either modality is unavailable in the test phase. Kampffmeyer et al. [35], therefore, proposed a hallucination network aiming to replace missing modalities during testing. Besides, enhancing the segmentation accuracy by optimizing object boundaries is another burgeoning research area [36,37].

The accuracy of FCN-based networks, although encouraging, appears to be incompetent for VFR segmentation. The reason is that almost all FCN-based networks are built on DCNNs, while the latter is designed for extracting local patterns and lacks the ability to model global context in its nature [38]. Hence, extensive investigations have been devoted to addressing the above issue since the long-range dependency is vital for segmenting confusing manmade objects in urban areas. Typical methods include dilated convolutional networks which are designed for enlarging the receptive field [39,40] and attentional networks that are proposed for capturing long-range relational semantic content of feature maps [30,41]. Nevertheless, these two networks have never been able to get rid of the dependence on the convolution operation, impairing the effectiveness of long-range information extraction.

Most recently, with its strong ability in long-range dependency capture and sequence-based image modelling, an entirely novel architecture named Transformer [42] has become prominent in various computer vision tasks, such as image classification [43], object detection [44], and semantic segmentation [45]. Transformer splits the input image into non-overlapping sequential patches and constructs feature extraction blocks consisting of multi-head self-attention (MHSA) and multilayer perceptron (MLP) to capture long-range dependencies [46]. Benefiting from the non-convolution structure and attention mechanism, Transformer could capture long-range dependencies more effectively [45,47].

Inspired by the advancement of Transformer, in this paper, we propose a bilateral awareness network (BANet) for accurate semantic segmentation of VFR urban scene images. Different from the traditional single-path convolutional neural networks, BANet addresses the challenging urban scene segmentation by constructing two feature extraction paths, as illustrated in Figure 1. Specifically, a texture path using stacked convolution layers is developed to extract the textural feature. Meanwhile, a dependency path using Transformer blocks is established to capture the long-range dependent feature. To leverage the benefits provided by the two features, we design a feature aggregation module (FAM) which introduces the linear attention mechanism to reduce the fitting residual of fused features, thereby strengthening the generalization capability of the network. Experimental results on three large-scale urban scene image segmentation datasets demonstrate the effectiveness of our BANet. Besides, the well-designed bilateral structure could provide a unified solution for semantic segmentation, object detection, and change detection, which undoubtedly boosts deep learning techniques in the remote sensing domain. To sum up, the main contributions of this paper are the following:

- (1) A novel bilateral structure composed of convolution layers and transformer blocks is proposed for understanding and labelling very fine resolution urban scene images. It provides a new perspective for capturing textural information and long-range dependencies simultaneously in a single network.
- (2) A feature aggregation module is developed to fuse the textural feature and longrange dependent feature extracted by the bilateral structure. It employs linear attention to reduce the fitting residual and greatly improves the generalization of fused features.

The remainder of this paper is organized as follows. The architecture of BANet and its components are detailed in Section 2. Experimental comparisons on three semantic segmentation datasets (UAVid, ISPRS Vaihingen, and Potsdam) are provided in Section 3. A comprehensive discussion is presented in Section 4. Finally, conclusions are drawn in Section 5.

## 2. Bilateral Awareness Network

#### 2.1. Overview

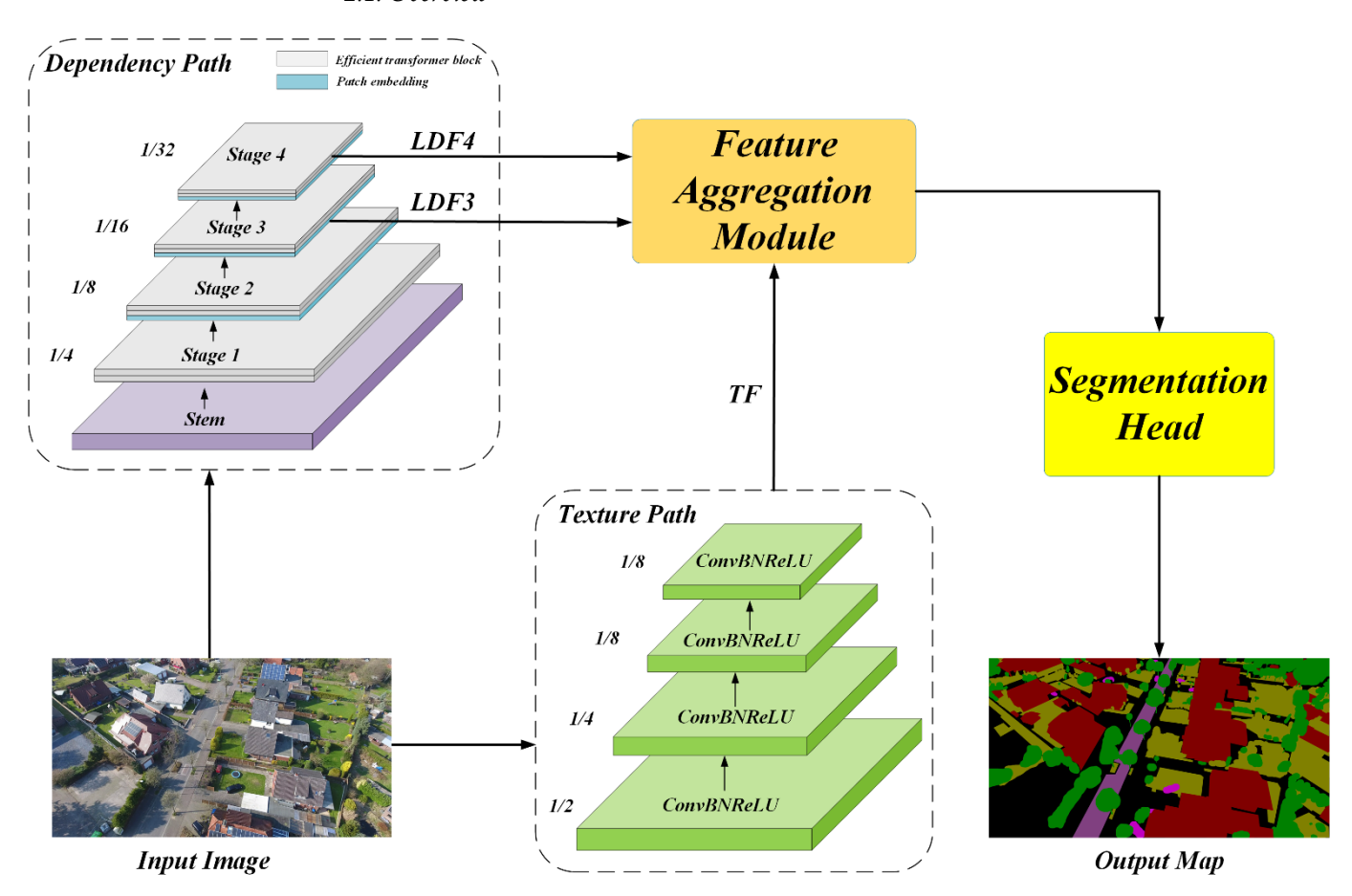


**Figure 1.** The overall architecture of BANet.

The overall architecture of the Bilateral Awareness Network (BANet) can be seen in Figure 1, where the input image is fed into the dependency path and texture path simultaneously.

The dependency path employs a stem block and four Transformer stages (i.e., Stage 1-4) to extract long-range dependent features (i.e., LDF3 and LDF4). Each stage consists of two stacked efficient transformer blocks (grey). In particular, Stage 2, Stage 3, and Stage 4 involve a patch embedding layer (blue) additionally. Proceed by the dependency path, the output two features are abundant with long-range dependencies.

The texture path deploys four convolutional layers to capture textural features (TF), while each convolutional layer is equipped with a batch normalization (BN) operation and a ReLU activation function. The downsampling factor is set as 8 for the texture path to preserve spatial details.

As the outputs of the dependency path (i.e., LDF3 and LDF4) and the output of the texture path (i.e., TF) are in disparate domains, a feature aggregation module (FAM) is proposed to effectively merge them. Whereafter, a segmentation head module is attached to convert the fused feature into a segmentation map.

## 2.2. Dependency path

The dependency path is constructed by the ResT-Lite [48] pertained on ImageNet. As an efficient vision transformer, ResT-Lite is suitable for urban scene interpretation due to its balanced trade-off between segmentation accuracy and computational complexity. The main basic modules of the ResT-lite include the stem block, patch embedding layer and efficient transformer block.

Stem block: The stem block is designed to shrink the height and width dimension and expand the channel dimension. To capture low-level information effectively, it introduces three  $3\times3$  convolution layers with strides of [2, 1, 2]. The first two convolution layers are followed by a Batch Normalization and ReLU activation. Proceed by the stem block, the spatial resolution is downscaled by a factor of 4, and the channel dimension is extended from 3 to 64.

*Patch embedding layer:* The patch embedding layer is developed to down-sampled the feature map for hierarchical feature representation. The output for each patch embedding layer can be formalized as:

$$PE(\mathbf{x}') = Sigmoid(DWConv(\mathbf{x}')) \cdot \mathbf{x}'$$
(1)

$$\mathbf{x}' = \mathrm{BN}(\mathbf{W}_{\mathbf{s}} \cdot \mathbf{x}) \tag{2}$$

where  $\mathbf{x}$  and  $\mathbf{x}'$  denote the feature map.  $W_s$  represents a convolution layer with a kernel size of s+1 and a stride of s. To obtain hierarchical feature representation, the hyperparameter s is set as 2. DWConv denotes a  $3\times3$  depth-wise convolution with a stride of 1.

Efficient transformer block: Each efficient transformer is composed of an efficient multihead self-attention (EMSA), a multilayer perceptron (MLP), and layer norm [49] operations. The output for each efficient transformer can be formalized as:

$$ET(\mathbf{x}) = G(\mathbf{x}) + MLP(LN(G(\mathbf{x})))$$
(3)

$$G(\mathbf{x}) = \mathbf{x} + \text{EMSA}(P(\mathbf{x})) \tag{4}$$

$$EMSA(\mathbf{Q}, \mathbf{K}, \mathbf{V}) = IN \left( Softmax \left( Conv \left( \frac{\mathbf{Q}\mathbf{K}^{T}}{\sqrt{d_k}} \right) \right) \cdot \mathbf{V} \right)$$
 (5)

Here, P is a combined function to obtain the three vectors (e.g.  $\mathbf{Q}$ ,  $\mathbf{K}$ ,  $\mathbf{V}$ ) using a linear project, a depth-wise convolution, and a Layer Normalization operation. Conv is a standard  $1\times1$  convolution with a stride of 1. IN denotes the Instance Normalization.  $d_k$  represents the head dimension. More details about EMSA can be seen in [48].

# 2.3. Texture path

The texture path is a lightweight convolutional network, which builds four diverse convolutional layers to capture textural information. The output for the texture path can be formalized as:

$$TF(\mathbf{x}) = T_4 \left( T_3 \left( T_2 (T_1(\mathbf{x})) \right) \right) \tag{6}$$

Here,  $\mathbf{x}$  is the input image vector. T represents a combined function consisting of a convolutional layer, a batch normalization operation, and a ReLU activation. The convolutional layer of  $T_1$  has a kernel size of 7 and a stride of 2, which expands the channel dimension from 3 to 64. For  $T_2$  and  $T_3$ , the kernel size and stride are 3 and 2, respectively. The channel dimension is kept as 64. For  $T_4$ , the convolutional layer is a standard  $1\times 1$  convolution with a stride of 1, expanding the channel dimension from 64 to 128. Thus, the output textural feature is downscaled 8 times and has a channel dimension of 128.

# 2.4. Feature aggregation module

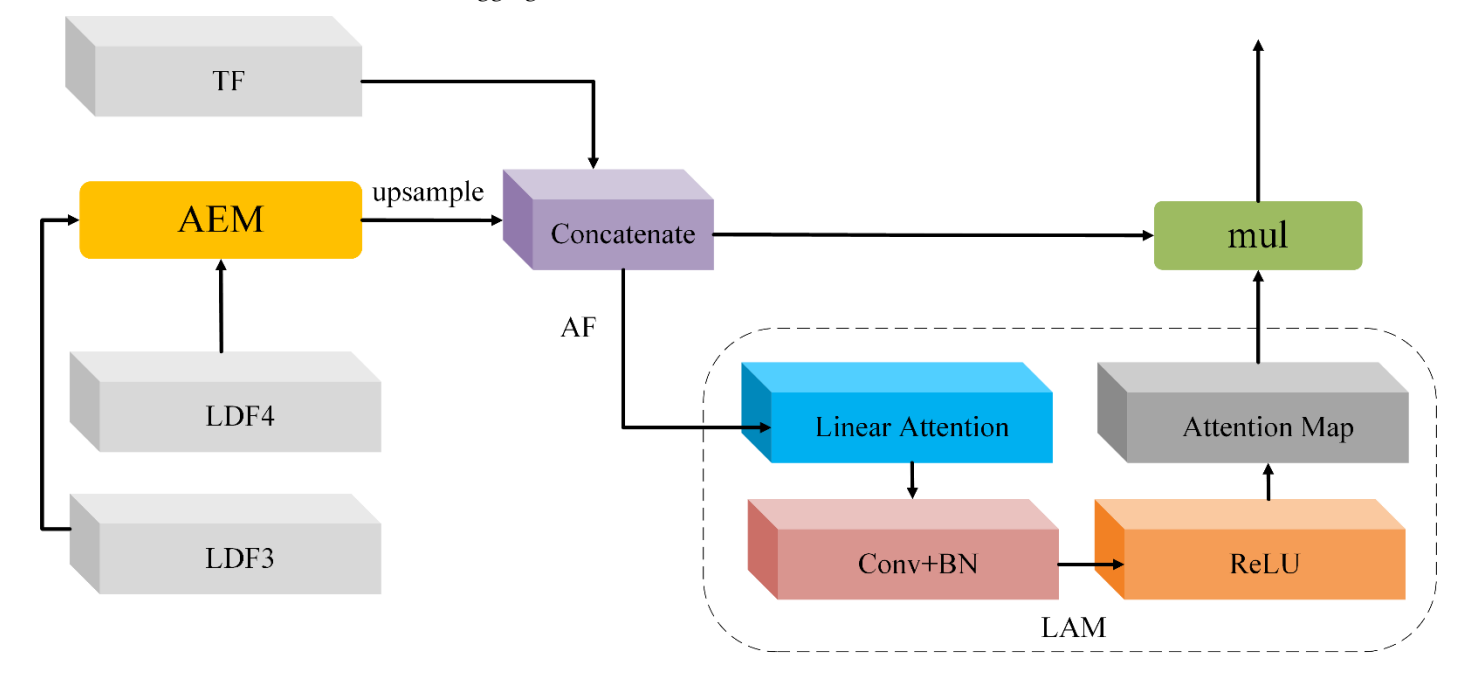


**Figure 2.** The feature aggregation module.

The aim of the feature aggregation module (FAM) is to leverage the benefits of the dependent features and texture features comprehensively for powerful feature representation. As shown in Figure 2, the input features for FAM include the long-range dependent features (LDF3 and LDF4) and the textural feature (TF). To fuse those features, we first employ an attentional embedding module (AEM) to merge the LDF3 and LDF4. Thereafter, the merged feature is up-sampled to concatenate with the TF, obtaining the aggregated feature (AF). Finally, the linear attention module (LAM) is deployed to reduce the fitting residual of AF. The pipeline of FAM can be denoted as:

$$FAM(AF) = AF \cdot LAM(AF)$$
 (7)

$$AF(TF, LDF3, LDF4) = C(U(AEM(LDF3, LDF4)), TF)$$
(8)

Here, C represents the concatenate function. U denotes an upsampling operation with a scale factor of 2. The detail of AEM and LAM are as follows.

Linear attention module (LAM): The linear attention module employs the linear attention (LA) mechanism to enhance the spatial relationships of AF, thereby suppressing the fitting residual. Then, a standard  $1\times1$  convolutional layer with batch normalization and ReLU activation is deployed to obtain the attention map. Finally, we apply a matrix multiplication operation between AF and the attention map to obtain the attentional AF. The linear attention mechanism is illustrated in Figure 3, which can be formalized as:

$$LAM(\mathbf{X}) = ConvBNReLU(LA(\mathbf{X}))$$
(9)

$$LA(\mathbf{X}) = \frac{\sum_{n} V(\mathbf{X})_{c,n} + \left(\frac{Q(\mathbf{X})}{\|Q(\mathbf{X})\|_{2}}\right) \left(\left(\frac{K(\mathbf{X})}{\|K(\mathbf{X})\|_{2}}\right)^{T} V(\mathbf{X})\right)}{N + \left(\frac{Q(\mathbf{X})}{\|Q(\mathbf{X})\|_{2}}\right) \sum_{n} \left(\frac{K(\mathbf{X})}{\|K(\mathbf{X})\|_{2}}\right)_{c,n}^{T}}$$
(10)

where Q, K and V in equation (10) represent the standard  $1 \times 1$  convolutional layer with a stride of 1. More details about the linear attention mechanism can be seen in our previous work [50].

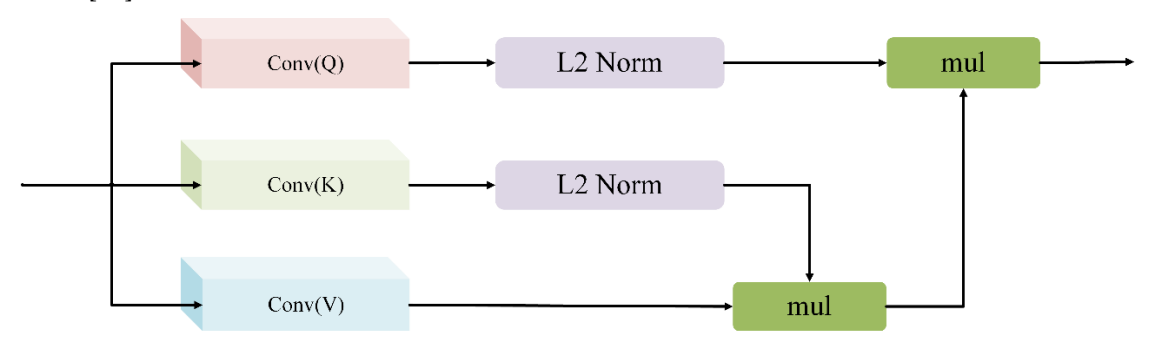


Figure 3. Linear attention.

Attentional embedding module (AEM): The attentional embedding module adopts the linear attention (LAM) module to enhance the spatial relationships of high-level semantic feature LDF4. Then, we apply a matrix multiplication operation between the upsampling attention map of LDF4 and LDF3. Finally, we use an addition operation to fuse the original LDF3 and the attentional LDF3. The pipeline of attentional embedding module is illustrated in Figure 4 and can be formalized as:

$$AEM(LDF3, LDF4) = LDF3 + LDF3 \cdot U(LAM(LDF4))$$
(11)

where U denotes the nearest upsampling operation with a scale factor of 2.

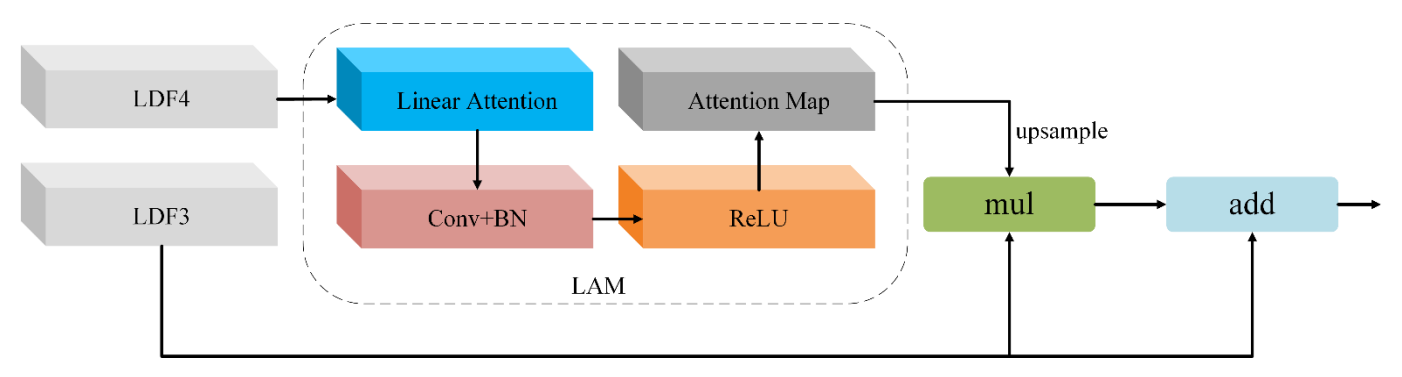


Figure 4. The attentional embedding module.

Capitalising on the benefits provided by linear attention and feature fusion, the final segmentation feature is abundant in both long-range dependency and textural information, demonstrating great generalization for precise semantic segmentation of urban scene images.

# 3. Experiments

In this section, experiments are conducted on two publicly available datasets to evaluate the effectiveness of the proposed BANet. We not only compare the performance of our model on the ISPRS Vaihingen and Potsdam datasets

(http://www2.isprs.org/commissions/comm3/wg4/semantic-labeling.html) against the state-of-the-art models designed for remote sensing images but also take those proposed for natural images into consideration. Further, the UAVid dataset [51] is utilized to demonstrate the advantages of our method. Please note that as the backbone for the dependency path of our BANet is ResT-Lite with 10.49 M parameters, the backbone for comparative methods is selected as ResNet-18 with 11.7 M parameters correspondingly for a fair comparison.

## 3.1. Experiments on the ISPRS Vaihingen and Potsdam Datasets

#### 3.1.1. Datasets

**Vaihingen**: There are 33 VFR images with a 2494 × 2064 average size in the Vaihingen dataset. The ground sampling distance (GSD) of tiles in Vaihingen is 9 cm. We utilize tiles: 2, 4, 6, 8, 10, 12, 14, 16, 20, 22, 24, 27, 29, 31, 33, 35, 38 for testing, tile: 30 for validation, and the remaining 15 images for training. Please note that we use only the near-infrared, red, and green channels in our experiments. The example images and labels can be seen in the top part of Figure 5.

**Potsdam**: There are 38 fine-resolution images that cover urban scenes in the size of  $6000 \times 6000$  pixels with a 5 cm GSD. We utilize ID: 2\_13, 2\_14, 3\_13, 3\_14, 4\_13, 4\_14, 4\_15, 5\_13, 5\_14, 5\_15, 6\_13, 6\_14, 6\_15, 7\_13 for testing, ID: 2\_10 for validation, and the remaining 22 images, except image named 7\_10 with error annotations, for training. Only the red, green, and blue channels are used in our experiments. The example images and labels can be seen in the bottom part of Figure 5.

## 3.1.2. Training Setting

For optimizing the network, the Adam is set as the optimizer with the 0.0003 learning rate and 8 batch size. The images, as well as corresponding labels, are cropped into patches with  $512 \times 512$  pixels and augmented by rotating, resizing, and flipping during training. All the experiments are implemented on a single NVIDIA RTX 3090 GPU with 24 GB RAM. The cross-entropy loss function is utilized as the loss function to measure the disparity between the achieved segmentation maps and the ground reference.

#### 3.1.3. Evaluation Metrics

The performance of BANet on the ISPRS Potsdam dataset is evaluated using the overall accuracy (OA), the mean Intersection over Union (mIoU), and the F1 score (F1), which are computed on the accumulated confusion matrix:

$$OA = \frac{\sum_{k=1}^{N} TP_k}{\sum_{k=1}^{N} TP_k + FP_k + TN_k + FN_k},$$
(12)

$$mIoU = \frac{1}{N} \sum_{k=1}^{N} \frac{TP_k}{TP_k + FP_k + FN_k'}$$
 (13)

$$F1 = 2 \times \frac{precision \times recall}{precision + recall'}$$
 (14)

where  $TP_k$ ,  $FP_k$ ,  $TN_k$ , and  $FN_k$  indicate the true positive, false positive, true negative, and false negatives, respectively, for object indexed as class k. OA is calculated for all categories including the background.

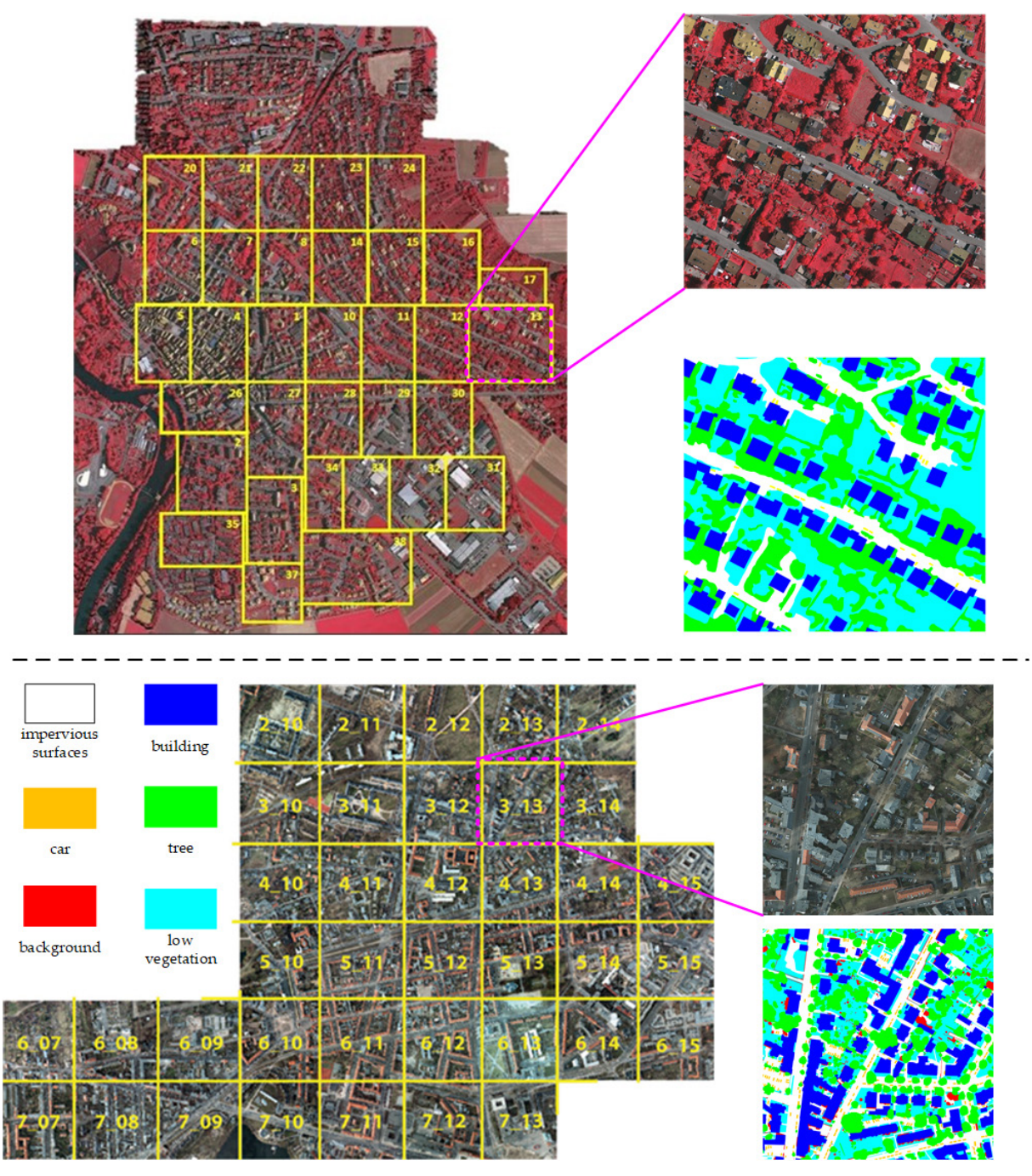


**Figure 5**. Example images and labels from the ISPRS Vaihingen dataset (top part) and Potsdam dataset (bottom part).

# 3.1.4. Experimental Results

A detailed comparison between our BANet and other architectures including BiSeNet [52], FANet [53], MAResU-Net [50], EaNet [36], SwiftNet [54], and ShelfNet [55] can be seen in Table 1 and Table 2, based upon the F1-score for each category, mean F1-score, and the OA, and the mIoU on the Potsdam test sets. As it can be observed from the table, the proposed BANet transcends the previous methods designed for segmentation by a large margin, achieving the highest OA of 90.28% and mIoU of 80.64% in the Vaihingen dataset, while the figures for the Potsdam dataset are 91.06% and 86.25%, respectively. Specifically, on the Vaihingen dataset, the proposed BANet brings more than 0.4% improvement in OA and 1.7% improvement in mIoU compared with the suboptimal method, while the improvements for the Potsdam dataset are more than 1.1% and 1.8%. Particularly, as the relatively small objects, the Car is difficult to recognize in the

Vaihingen dataset. Even so, the proposed BANet achieves a 86.76% F1-score, preceding the suboptimal method by more than 5.5%.

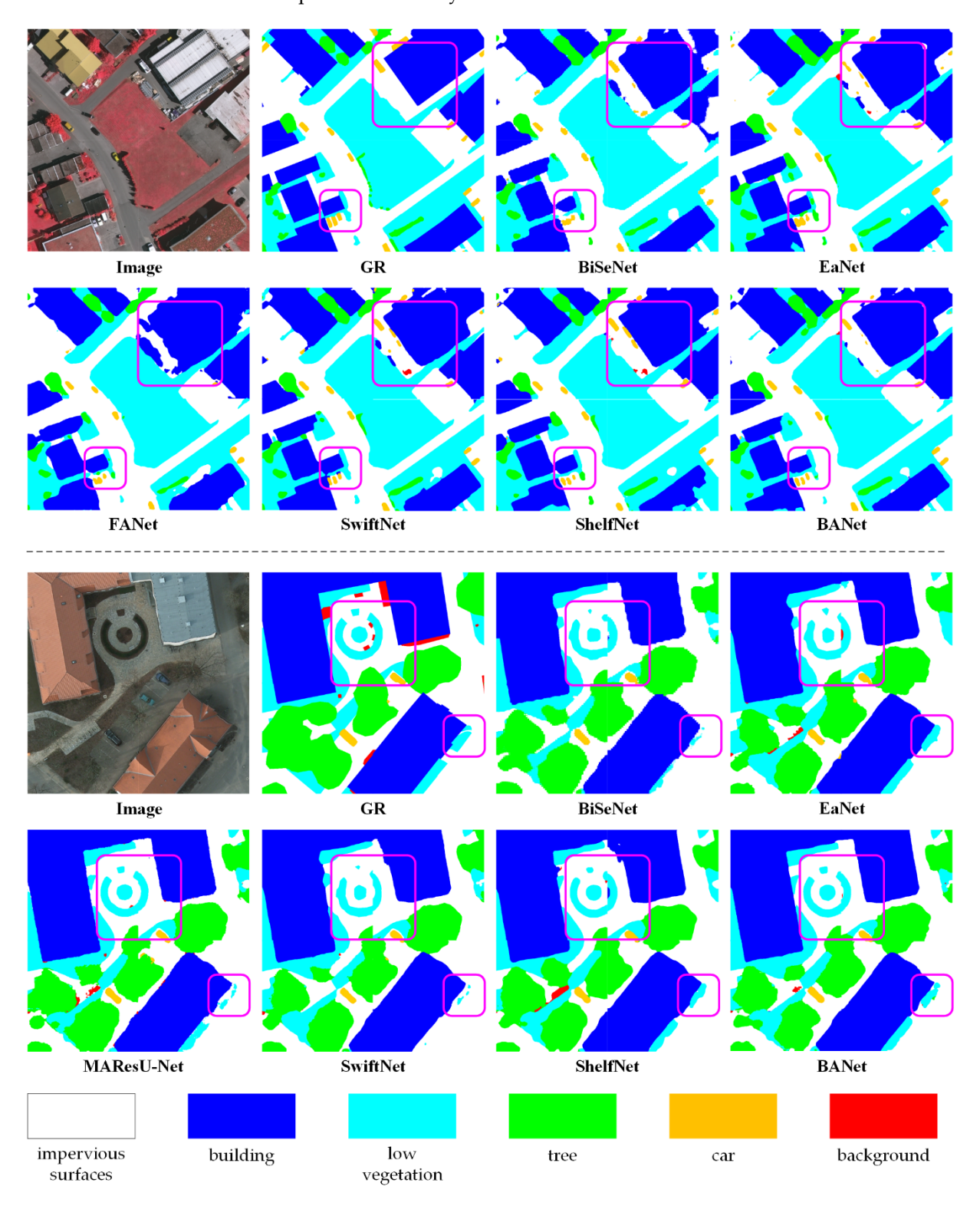


**Figure 6**. The experimental results on the ISPRS Vaihingen dataset (top part) and Potsdam dataset (bottom part).

To qualitatively validate the effectiveness, we visualise the segmentation maps generated by our BANet and comparative methods in Figure 6. Due to the limited receptive field, the BiSeNet, EaNet, and SwiftNet assign the classification of a specific pixel only by considering a few adjacent areas, leading to fragmented maps and confusion of

objects. The direct utilization of the attention mechanism (i.e., MAResU-Net) and the structure of multiple encoder-decoder (i.e., ShelfNet) brings certain improvements. However, the issue of the receptive field is still not entirely resolved. By contrast, we construct the dependency path in our BANet based on an attention-based backbone, i.e., ResT, to capture the long-range global relations, thereby tackling the limitation of the receptive field. Furthermore, a texture path built on convolution operation is equipped in our BANet to utilize the spatial details information in feature maps. Particularly, as shown in Figure 6, the complex circular contour of the Low vegetation is preserved completely by our BANet. Besides, the outlines of the Building generated by our BANet are more smooth than those obtained by comparative methods.

Table 1. The experimental results on the Vaihingen dataset.

Method	Backbone	Imp. surf.	Building	Low veg.	Tree	Car	Mean F1	OA	mIoU
BiSeNet	ResNet-18	89.12	91.30	80.87	86.91	73.12	84.26	87.08	75.82
FANet	ResNet-18	90.65	93.78	82.60	88.56	71.60	85.44	88.87	75.61
MAResU-Net	ResNet-18	91.97	95.04	83.74	89.35	78.28	87.68	90.07	78.58
EaNet	ResNet-18	91.68	94.52	83.10	89.24	79.98	87.70	89.69	78.68
SwiftNet	ResNet-18	92.22	94.84	84.14	89.31	81.23	88.35	90.20	79.58
ShelfNet	ResNet-18	91.83	94.56	83.78	89.27	77.91	87.47	89.81	78.94
BANet	ResT-Lite	92.23	95.23	83.75	89.92	86.76	89.57	90.48	81.35

**Table 2.** The experimental results on the Potsdam dataset.

Method	Backbone	Imp. surf.	Building	Low veg.	Tree	Car	Mean F1	OA	mIoU
BiSeNet	ResNet-18	90.24	94.55	85.53	86.20	92.68	89.84	88.16	81.72
<b>FANet</b>	ResNet-18	91.99	96.10	86.05	87.83	94.53	91.30	89.82	84.16
MAResU-Net	ResNet-18	91.41	95.57	85.82	86.61	93.31	90.54	89.04	83.87
EaNet	ResNet-18	92.01	95.69	84.31	85.72	95.11	90.57	88.70	83.38
SwiftNet	ResNet-18	91.83	95.94	85.72	86.84	94.46	90.96	89.33	83.84
ShelfNet	ResNet-18	92.53	95.75	86.60	87.07	94.59	91.31	89.92	84.38
BANet	ResT-Lite	93.34	96.66	87.37	89.12	95.99	91.98	91.06	86.25

# 3.2. Experiments on the UAVid Dataset

# 3.2.1. Dataset

As a fine-resolution Unmanned Aerial Vehicle (UAV) semantic segmentation dataset, the UAVid dataset (<a href="https://uavid.nl/">https://uavid.nl/</a>) is focusing on urban street scenes with a  $3840 \times 2160$  resolution. UAVid is a challenging benchmark since the large resolution of images, large-scale variation, and complexities in the scenes. To be specific, there are 420 images in the dataset where 200 are for training, 70 for validation, and the remaining 150 for testing. The example images and labels can be seen in Figure 7.

We adopt the same hyperparameters and data augmentation as those for experiments on the ISPRS Potsdam dataset, except batch size as 4 and the patch size as  $1024 \times 1024$  during training.

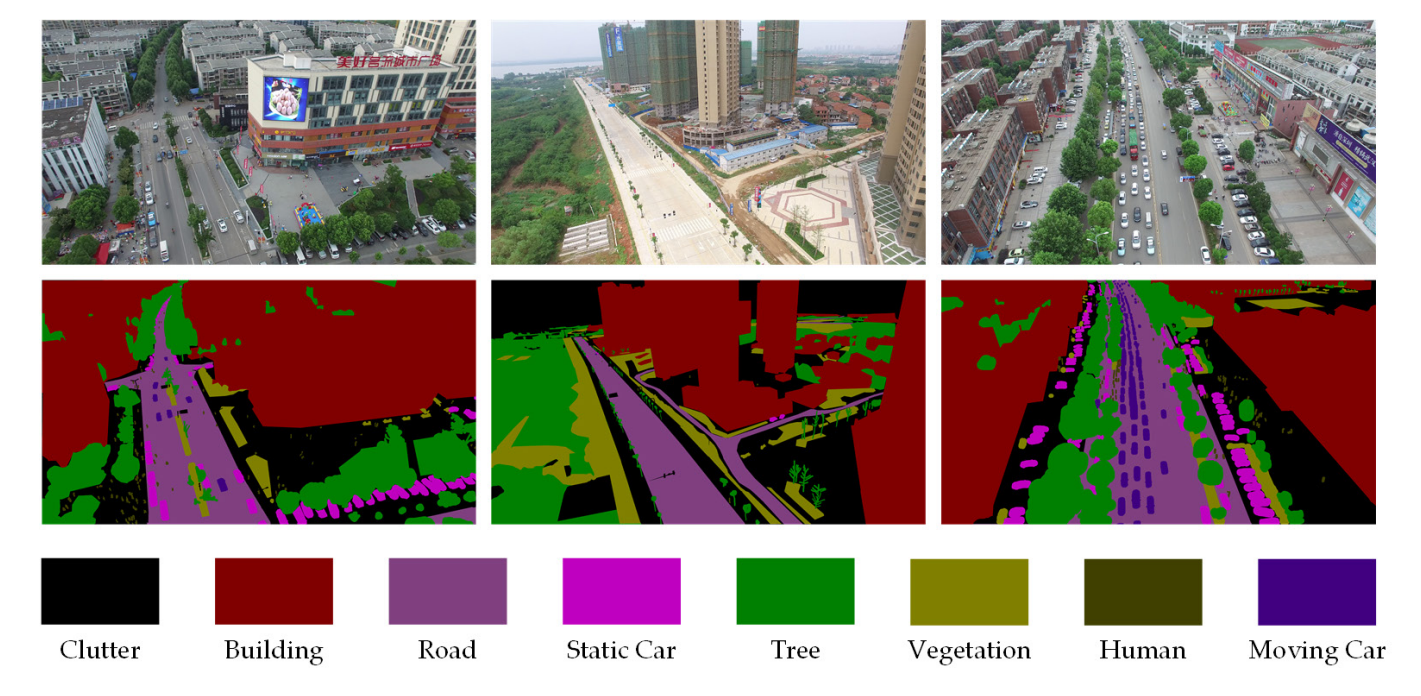


Figure 7. Example images and labels from the UAVid dataset.

# 3.2.2. Evaluation Metrics

For the UAVid dataset, the performance is assessed from the official server based on the intersection-over-union metric:

$$IoU = \frac{TP_k}{TP_k + FP_k + FN_k},\tag{15}$$

where  $TP_k$ ,  $FP_k$ ,  $TN_k$ , and  $FN_k$  indicate the true positive, false positive, true negative, and false negatives, respectively, for object indexed as class k.

# 3.2.3. Experimental Results

Quantitative comparison with MSD [51], Fast-SCNN [56], BiSeNet [52], SwiftNet [54] and ShelfNet [55] are reported in Table 3. As can be seen, the proposed BANet achieves the best IOU score on five out of eight classes, and the best mIoU with a 3% gain over the suboptimal BiSeNet. Qualitative results on the UAVid validation set and test set are demonstrated in Figure 8 and Figure 9, respectively. Compared with the benchmark MSD with obvious local and global inconsistencies, the proposed BANet can effectively capture the cues to scene semantics. For example, in the second row of Figure 9, the cars in the pink box are obviously all moving on the road. However, the MSD identity the left car which is crossing the street as the static car. In contrast, our BANet successfully recognizes all moving cars.

<b>Table 3</b> . The experimental 1	results on the	· UAVid dataset.
-------------------------------------	----------------	------------------

Method	building	tree	clutter	road	vegetation	static car	moving car	human	mIoU
MSD	79.8	74.5	57.0	74.0	55.9	32.1	62.9	19.7	57.0
Fast-SCNN	75.7	71.5	44.2	61.6	43.4	19.5	51.6	0.0	45.9
BiSeNet	85.7	78.3	64.7	61.1	77.3	63.4	48.6	17.5	61.5
SwiftNet	85.3	78.2	64.1	61.5	76.4	62.1	51.1	15.7	61.1
ShelfNet	76.9	73.2	44.1	61.4	43.4	21.0	52.6	3.6	47.0
BANet	85.4	78.9	66.6	80.7	62.1	52.8	69.3	21.0	64.6

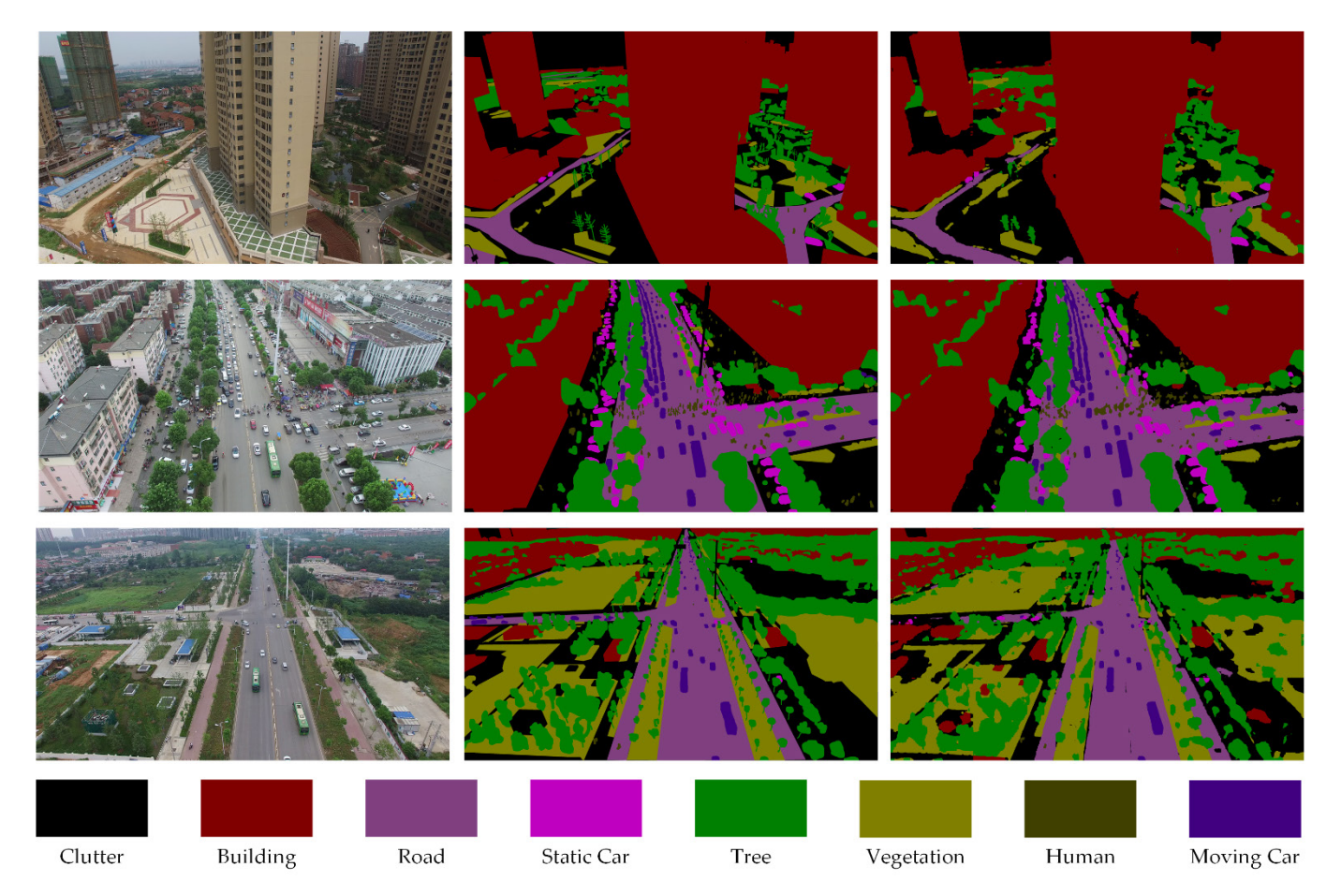


**Figure 8**. The experimental results on the UAVid validation set. The first column illustrates the input RGB images, the second column depicts the ground reference and the third column shows the predictions of our BANet.

## 4. Discussion

In this part, we conduct extensive ablation experiments to verify the effectiveness of components in the proposed BANet, while the experimental settings and quantitative comparisons are illustrated in Table 4.

**Baseline**: We select two baselines in ablation experiments, the dependency path which utilizes the ResNet-18 (denoted as ResNet) as the backbone and the dependency path which adopts the ResT-Lite (denoted as ResT) as the backbone. The feature maps generated by the dependency path are directly up-sampled to restore the shape for final segmentation.

**Ablation for the texture path**: As rich spatial details are important for segmentation, the texture path conducted on the convolution operation is designed in our BANet for preserving the spatial texture. Table 3 illustrates that even the simple fusion schemes such as summation (indicated as Dp+Tp(Sum)) and concatenation (signified as Dp+Tp(Cat)) to merge the texture information can enhance the performance in OA at least 0.3%.

**Ablation for feature aggregation module**: Given the information obtained by the dependency path and the texture path are in different domains, neither summation nor concatenation is the optimal feature fusion scheme. As shown in Table 3, more than 0.6% improvement in OA brings by our BANet compared with Dp+Tp(Sum) and Dp+Tp(Cat) explains the validity of the proposed feature aggregation module.

**Ablation for ResT-Lite**: Since a novel transformer-based backbone, i.e., ResT, is introduced in our BANet, it is valuable to compare the accuracy between the ResNet and ResT. As illustrated in Table 3, the replacement of the backbone in the dependency path brings more than the 1% improvement in OA. Besides, we substitute the backbone in our

BANet with ResNet-18 (denoted as BAResNet) to further evaluate the performance. As can be seen in Table 3, a 0.8% gap in OA illuminates the effectiveness of the ResT-Lite.

Method	Imp. surf.	Building	Low veg.	Tree	Car	Mean F1	OA	mIoU
ResNet	91.41	95.57	85.82	86.61	93.31	90.54	89.04	82.94
ResT	92.63	96.48	86.34	87.65	94.61	91.54	90.06	84.65
Dp+Tp(Sum)	92.66	96.08	87.05	87.99	94.69	91.69	90.37	84.87
Dp+Tp(Cat)	92.93	96.42	86.88	88.39	95.45	92.01	90.54	85.44
BAResNet	92.70	95.78	86.76	87.97	95.00	91.64	90.20	84.78
BANet	93.34	96.66	87.37	89.12	95.99	91.98	91.06	86.25

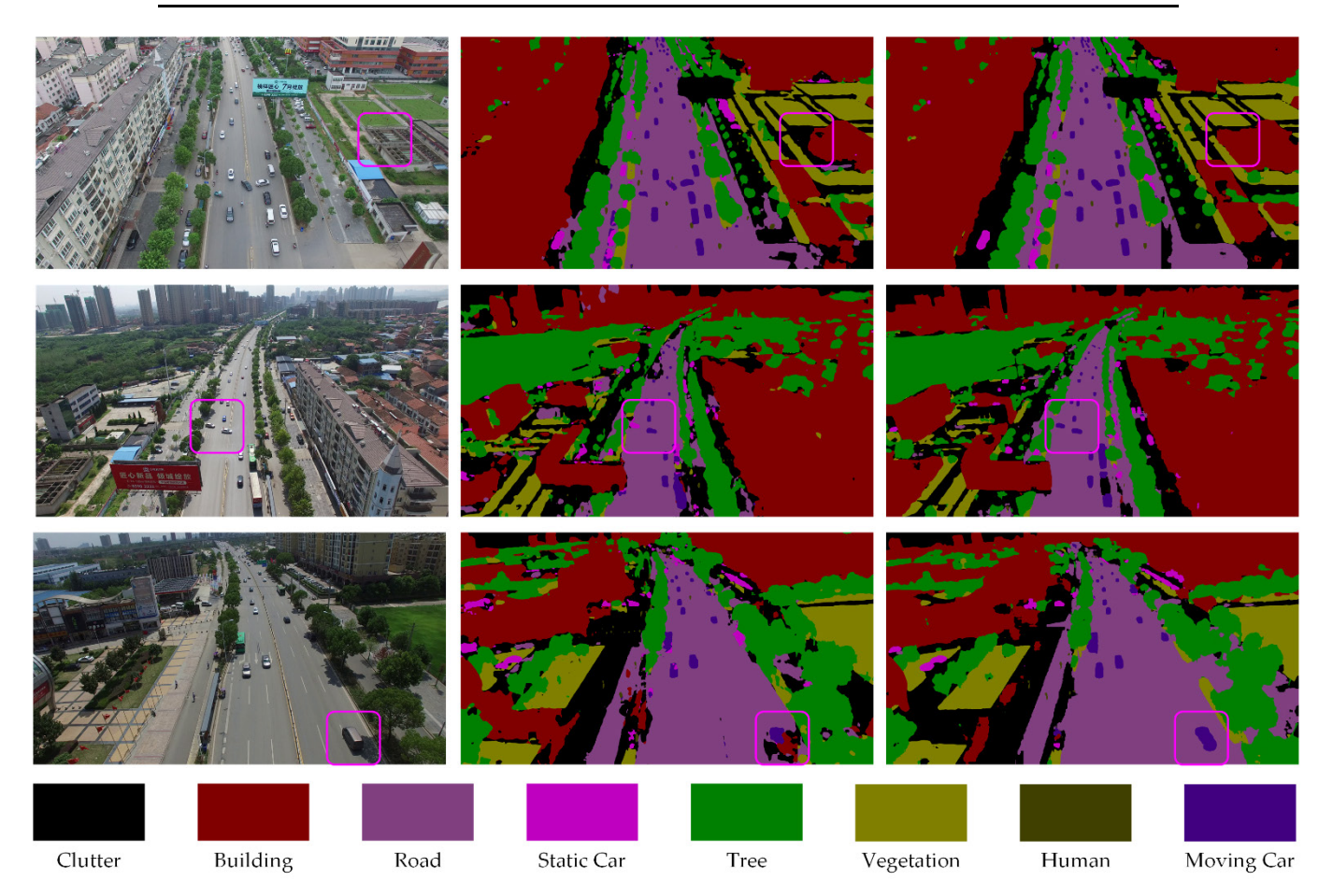


**Figure 9**. The experimental results on the UAVid test set. The first column illustrates the input RGB images, the second column depicts the outputs of MSD and the third column shows the predictions of our BANet.

#### 5. Conclusions

This paper proposes a Bilateral Awareness Network (BANet) for semantic segmentation of very fine resolution urban scene images. Specifically, there are two branches in our BANet, a dependency path built on the Transformer backbone to capture the long-range relationships and a texture path constructed on the convolution operation to exploit the fine-grained details in VHR images. In particular, we further design an attention aggregation module to fuse the global relationship information captured by the dependency path and the spatial texture information generated by the texture path. Extensive experiments on the ISPRS Vaihingen dataset, ISPRS Potsdam dataset, and UAVid dataset demonstrate the effectiveness of the proposed BANet. As a novel

exploration to combine the Transformer and convolution in a bilateral structure, we envisage this pioneering paper could inspire practitioners and researchers engaged in this area to explore more possibilities of the Transformer in the remote sensing domain.

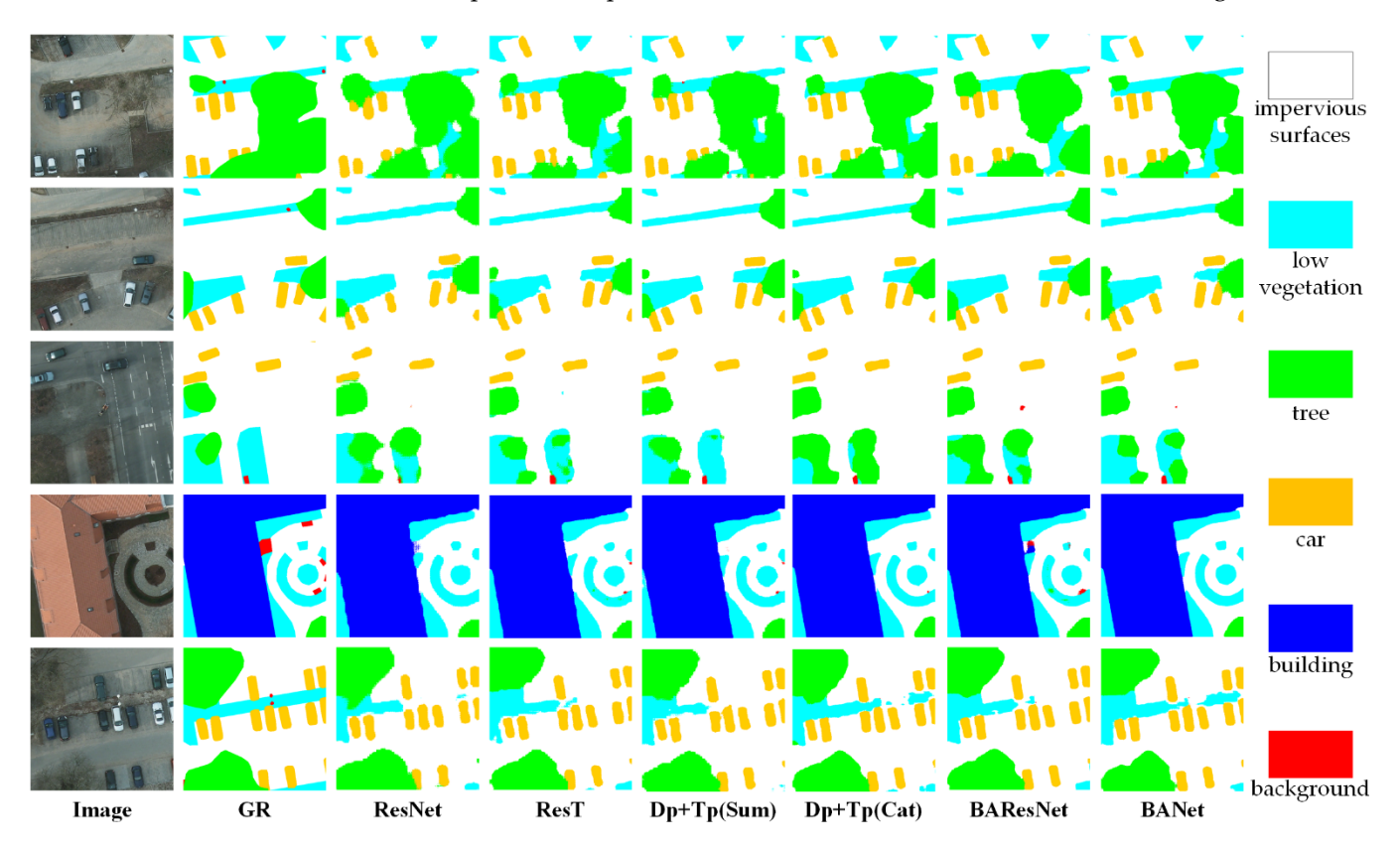


Figure 10. The ablation study on the ISPRS Potsdam dataset. GR represents Ground Reference.

**Author Contributions:** This work was conducted in collaboration with all author. Dongzhi Wang and Teng Wang defined the research theme. Xiaoliang Meng supervised the research work and provided experimental facilities. Libo Wang and Rui Li designed the semantic segmentation model and conducted the experiments. Chenxi Duan checked the experimental results. This manuscript was written by Libo Wang and Rui Li. All authors have read and agreed to the published version of the manuscript.

**Funding:** This research was funded by the National Natural Science Foundation of China (NSFC) under grant number 41971352, National Key Research and Development Program of China under grant number 2018YFB0505003.

**Acknowledgements**: The authors are very grateful to the many people who helped to comment on the article, and the Large Scale Environment Remote Sensing Platform (Facility No. 16000009, 16000011, 16000012) provided by Wuhan University. Special thanks to editors and reviewers for providing valuable insight into this article.

Data Availability Statement: We are grateful to ISPRS for providing the open benchmarks for 2D remote sensing image semantic segmentation. The data in the paper can be obtained through the following link: <a href="https://www2.isprs.org/commissions/comm2/wg4/benchmark/2d-sem-label-potsdam/">https://www2.isprs.org/commissions/comm2/wg4/benchmark/2d-sem-label-potsdam/</a> and <a href="https://www2.isprs.org/commissions/comm2/wg4/benchmark/2d-sem-label-vaihingen/">https://www2.isprs.org/commissions/comm2/wg4/benchmark/2d-sem-label-vaihingen/</a>.

**Conflicts of Interest:** The authors declare no conflict of interest.

#### **Abbreviations:**

The following abbreviations are used in this manuscript:

VFR Very Fine Resolution

DCNNs Deep Convolutional Neural Networks

FCN Fully Convolutional Neural Network

SVM Support Vector Machine

RF Random Forest

CRF Conditional Random Field MHSA Multi-Head Self-Attention MLP Multilayer Perceptron

FAM Feature Aggregation Module BANet Bilateral Awareness Network

TF Textural Features
AF Aggregated Features

LDF Long-range Dependent Features

BN Batch Normalization

GSD Ground Sampling Distance
UAV Unmanned Aerial Vehicle

LA Linear Attention

AEM Attentional Embedding Module EMSA Efficient Multi-head Self-attention

#### References

- 1. Zhang, C.; Atkinson, P.M.; George, C.; Wen, Z.; Diazgranados, M.; Gerard, F. Identifying and mapping individual plants in a highly diverse high-elevation ecosystem using UAV imagery and deep learning. *ISPRS Journal of Photogrammetry and Remote Sensing* **2020**, *169*, 280-291.
- 2. Zhang, C.; Harrison, P.A.; Pan, X.; Li, H.; Sargent, I.; Atkinson, P.M. Scale Sequence Joint Deep Learning (SS-JDL) for land use and land cover classification. *Remote Sensing of Environment* **2020**, 237, 111593.
- 3. Rui, L.; Cehnxi, D.; Shunyi, Z. MACU-Net Semantic Segmentation from High-Resolution Remote Sensing Images. *arXiv* preprint arXiv:2007.13083 **2020**.
- 4. Li, R.; Duan, C. ABCNet: Attentive Bilateral Contextual Network for Efficient Semantic Segmentation of Fine-Resolution Remote Sensing Images. *arXiv preprint arXiv:2102.02531* **2021**.
- 5. Wang, L.; Fang, S.; Zhang, C.; Li, R.; Duan, C.; Meng, X.; Atkinson, P.M. SaNet: Scale-aware Neural Network for Semantic Labelling of Multiple Spatial Resolution Aerial Images. *arXiv preprint arXiv:2103.07935* **2021**.
- 6. Huang, Z.; Wei, Y.; Wang, X.; Shi, H.; Liu, W.; Huang, T.S. Alignseg: Feature-aligned segmentation networks. *IEEE Transactions on Pattern Analysis and Machine Intelligence* **2021**.
- 7. Yao, H.; Qin, R.; Chen, X. Unmanned Aerial Vehicle for Remote Sensing Applications—A Review. *Remote Sensing* **2019**, 11, doi:10.3390/rs11121443.
- 8. Audebert, N.; Le Saux, B.; Lefèvre, S. Segment-before-Detect: Vehicle Detection and Classification through Semantic Segmentation of Aerial Images. *Remote Sensing* **2017**, *9*, doi:10.3390/rs9040368.
- 9. Matikainen, L.; Karila, K. Segment-Based Land Cover Mapping of a Suburban Area—Comparison of High-Resolution Remotely Sensed Datasets Using Classification Trees and Test Field Points. *Remote Sensing* **2011**, *3*, doi:10.3390/rs3081777.
- 10. Zhang, Q.; Seto, K.C. Mapping urbanization dynamics at regional and global scales using multi-temporal DMSP/OLS nighttime light data. *Remote Sensing of Environment* **2011**, *115*, 2320-2329, doi:https://doi.org/10.1016/j.rse.2011.04.032.
- 11. Wei, Y.; Wang, Z.; Xu, M. Road Structure Refined CNN for Road Extraction in Aerial Image. *IEEE Geoscience and Remote Sensing Letters* **2017**, *14*, 709-713, doi:10.1109/LGRS.2017.2672734.
- 12. Li, E.; Femiani, J.; Xu, S.; Zhang, X.; Wonka, P. Robust Rooftop Extraction From Visible Band Images Using Higher Order CRF. *IEEE Transactions on Geoscience and Remote Sensing* **2015**, *53*, 4483-4495, doi:10.1109/TGRS.2015.2400462.

- 13. Diakogiannis, F.I.; Waldner, F.; Caccetta, P.; Wu, C. ResUNet-a: A deep learning framework for semantic segmentation of remotely sensed data. *ISPRS Journal of Photogrammetry and Remote Sensing* **2020**, 162, 94-114, doi:https://doi.org/10.1016/j.isprsjprs.2020.01.013.
- 14. Li, R.; Zheng, S.; Duan, C.; Su, J. Multi-Attention-Network for Semantic Segmentation of High-Resolution Remote Sensing Images. *arXiv preprint arXiv:2009.02130* **2020**.
- Thang, C.; Sargent, I.; Pan, X.; Li, H.; Gardiner, A.; Hare, J.; Atkinson, P.M. Joint Deep Learning for land cover and land use classification. *Remote Sensing of Environment* **2019**, 221, 173-187, doi:https://doi.org/10.1016/j.rse.2018.11.014.
- Zhang, C.; Sargent, I.; Pan, X.; Li, H.; Gardiner, A.; Hare, J.; Atkinson, P.M. An object-based convolutional neural network 16. classification. (OCNN) for urban land use Remote Sensing of Environment 2018. 216. 57-70, doi:https://doi.org/10.1016/j.rse.2018.06.034.
- 17. LeCun, Y.; Bengio, Y.; Hinton, G. Deep learning. nature 2015, 521, 436-444.
- 18. Long, J.; Shelhamer, E.; Darrell, T. Fully convolutional networks for semantic segmentation. In Proceedings of Proceedings of the IEEE/CVF Conference on Computer Vision and Pattern Recognition, 2015; pp. 3431-3440.
- 19. Sherrah, J. Fully convolutional networks for dense semantic labelling of high-resolution aerial imagery. *arXiv preprint arXiv:1606.02585* **2016**.
- 20. Guo, Y.; Jia, X.; Paull, D. Effective Sequential Classifier Training for SVM-Based Multitemporal Remote Sensing Image Classification. *IEEE Transactions on Image Processing* **2018**, 27, 3036-3048, doi:10.1109/TIP.2018.2808767.
- 21. Pal, M. Random forest classifier for remote sensing classification. *International Journal of Remote Sensing* **2005**, *26*, 217-222, doi:10.1080/01431160412331269698.
- 22. Krähenbühl, P.; Koltun, V. Efficient inference in fully connected crfs with gaussian edge potentials. *Advances in neural information processing systems* **2011**, 24, 109-117.
- 23. Ma, L.; Liu, Y.; Zhang, X.; Ye, Y.; Yin, G.; Johnson, B.A. Deep learning in remote sensing applications: A meta-analysis and review. *ISPRS Journal of Photogrammetry and Remote Sensing* **2019**, *152*, 166-177, doi:https://doi.org/10.1016/j.isprsjprs.2019.04.015.
- 24. Marcos, D.; Volpi, M.; Kellenberger, B.; Tuia, D. Land cover mapping at very high resolution with rotation equivariant CNNs: Towards small yet accurate models. *ISPRS Journal of Photogrammetry and Remote Sensing* **2018**, *145*, 96-107, doi:https://doi.org/10.1016/j.isprsjprs.2018.01.021.
- 25. Ronneberger, O.; Fischer, P.; Brox, T. U-Net: Convolutional Networks for Biomedical Image Segmentation. In Proceedings of Medical Image Computing and Computer-Assisted Intervention MICCAI 2015, Cham, 2015//; pp. 234-241.
- Yue, K.; Yang, L.; Li, R.; Hu, W.; Zhang, F.; Li, W. TreeUNet: Adaptive Tree convolutional neural networks for subdecimeter aerial image segmentation. *ISPRS Journal of Photogrammetry and Remote Sensing* **2019**, *156*, 1-13, doi:https://doi.org/10.1016/j.isprsjprs.2019.07.007.
- 27. Li, R.; Duan, C.; Zheng, S.; Zhang, C.; Atkinson, P.M. MACU-Net for Semantic Segmentation of Fine-Resolution Remotely Sensed Images. *IEEE Geoscience and Remote Sensing Letters* **2021**, 10.1109/LGRS.2021.3052886, 1-5, doi:10.1109/LGRS.2021.3052886.
- 28. Liu, Y.; Fan, B.; Wang, L.; Bai, J.; Xiang, S.; Pan, C. Semantic labeling in very high resolution images via a self-cascaded convolutional neural network. *ISPRS journal of photogrammetry and remote sensing* **2018**, *145*, 78-95.
- 29. Li, R.; Zheng, S.; Duan, C.; Su, J.; Zhang, C. Multistage Attention ResU-Net for Semantic Segmentation of Fine-Resolution Remote Sensing Images. *IEEE Geoscience and Remote Sensing Letters* **2021**, 10.1109/LGRS.2021.3063381, 1-5, doi:10.1109/LGRS.2021.3063381.
- 30. Fu, J.; Liu, J.; Tian, H.; Li, Y.; Bao, Y.; Fang, Z.; Lu, H. Dual attention network for scene segmentation. In Proceedings of Proceedings of the IEEE/CVF Conference on Computer Vision and Pattern Recognition; pp. 3146-3154.

- 31. Zhao, H.; Qi, X.; Shen, X.; Shi, J.; Jia, J. Icnet for real-time semantic segmentation on high-resolution images. In Proceedings of Proceedings of the European conference on computer vision (ECCV), 2018; pp. 405-420.
- 32. Kampffmeyer, M.; Salberg, A.-B.; Jenssen, R. Semantic segmentation of small objects and modeling of uncertainty in urban remote sensing images using deep convolutional neural networks. In Proceedings of Proceedings of the IEEE conference on computer vision and pattern recognition workshops; pp. 1-9.
- 33. Maggiori, E.; Tarabalka, Y.; Charpiat, G.; Alliez, P. High-resolution aerial image labeling with convolutional neural networks. *IEEE Transactions on Geoscience and Remote Sensing* **2017**, *55*, 7092-7103.
- 34. Audebert, N.; Le Saux, B.; Lefèvre, S. Beyond RGB: Very high resolution urban remote sensing with multimodal deep networks. *ISPRS Journal of Photogrammetry and Remote Sensing* **2018**, 140, 20-32.
- 35. Kampffmeyer, M.; Salberg, A.-B.; Jenssen, R. Urban land cover classification with missing data modalities using deep convolutional neural networks. *IEEE Journal of Selected Topics in Applied Earth Observations and Remote Sensing* **2018**, *11*, 1758-1768.
- 36. Zheng, X.; Huan, L.; Xia, G.-S.; Gong, J. Parsing very high resolution urban scene images by learning deep ConvNets with edge-aware loss. *ISPRS Journal of Photogrammetry and Remote Sensing* **2020**, *170*, 15-28.
- 37. Marmanis, D.; Schindler, K.; Wegner, J.D.; Galliani, S.; Datcu, M.; Stilla, U. Classification with an edge: Improving semantic image segmentation with boundary detection. *ISPRS Journal of Photogrammetry and Remote Sensing* **2018**, *135*, 158-172.
- 38. Wang, X.; Girshick, R.; Gupta, A.; He, K. Non-local neural networks. In Proceedings of Proceedings of the IEEE conference on computer vision and pattern recognition; pp. 7794-7803.
- 39. Yu, F.; Koltun, V. Multi-scale context aggregation by dilated convolutions. arXiv preprint arXiv:1511.07122 2015.
- 40. Liu, Q.; Kampffmeyer, M.; Jenssen, R.; Salberg, A.B. Dense Dilated Convolutions' Merging Network for Land Cover Classification. *IEEE Transactions on Geoscience and Remote Sensing* **2020**, *58*, 6309-6320, doi:10.1109/TGRS.2020.2976658.
- 41. Huang, Z.; Wang, X.; Wei, Y.; Huang, L.; Shi, H.; Liu, W.; Huang, T.S. CCNet: Criss-Cross Attention for Semantic Segmentation. *IEEE Transactions on Pattern Analysis and Machine Intelligence* **2020**, 10.1109/TPAMI.2020.3007032, 1-1, doi:10.1109/TPAMI.2020.3007032.
- 42. Vaswani, A.; Shazeer, N.; Parmar, N.; Uszkoreit, J.; Jones, L.; Gomez, A.N.; Kaiser, L.; Polosukhin, I. Attention is all you need. arXiv preprint arXiv:1706.03762 2017.
- 43. Dosovitskiy, A.; Beyer, L.; Kolesnikov, A.; Weissenborn, D.; Zhai, X.; Unterthiner, T.; Dehghani, M.; Minderer, M.; Heigold, G.; Gelly, S. An image is worth 16x16 words: Transformers for image recognition at scale. *arXiv preprint arXiv:2010.11929* **2020**.
- 44. Zhu, X.; Su, W.; Lu, L.; Li, B.; Wang, X.; Dai, J. Deformable DETR: Deformable Transformers for End-to-End Object Detection. arXiv preprint arXiv:2010.04159 2020.
- 45. Wang, L.; Li, R.; Duan, C.; Fang, S. Transformer Meets DCFAM: A Novel Semantic Segmentation Scheme for Fine-Resolution Remote Sensing Images. *arXiv* preprint *arXiv*:2104.12137 **2021**.
- 46. Liang, J.; Homayounfar, N.; Ma, W.-C.; Xiong, Y.; Hu, R.; Urtasun, R. Polytransform: Deep polygon transformer for instance segmentation. In Proceedings of Proceedings of the IEEE/CVF Conference on Computer Vision and Pattern Recognition, 2020; pp. 9131-9140.
- 47. Liu, Z.; Lin, Y.; Cao, Y.; Hu, H.; Wei, Y.; Zhang, Z.; Lin, S.; Guo, B. Swin transformer: Hierarchical vision transformer using shifted windows. *arXiv preprint arXiv:2103.14030* **2021**.
- 48. Zhang, Q.; Yang, Y. ResT: An Efficient Transformer for Visual Recognition. arXiv preprint arXiv:2105.13677 2021.
- 49. Ghiasi, G.; Lin, T.-Y.; Le, Q.V. Nas-fpn: Learning scalable feature pyramid architecture for object detection. In Proceedings of Proceedings of the IEEE/CVF Conference on Computer Vision and Pattern Recognition, 2019; pp. 7036-7045.
- 50. Li, R.; Su, J.; Duan, C.; Zheng, S. Multistage Attention ResU-Net for Semantic Segmentation of Fine-Resolution Remote Sensing Images. *arXiv* preprint *arXiv*:2011.14302 **2020**.

- 51. Lyu, Y.; Vosselman, G.; Xia, G.-S.; Yilmaz, A.; Yang, M.Y. UAVid: A semantic segmentation dataset for UAV imagery. *ISPRS Journal of Photogrammetry and Remote Sensing* **2020**, *165*, 108-119.
- 52. Yu, C.; Wang, J.; Peng, C.; Gao, C.; Yu, G.; Sang, N. Bisenet: Bilateral segmentation network for real-time semantic segmentation. In Proceedings of Proceedings of the European conference on computer vision (ECCV); pp. 325-341.
- 53. Hu, P.; Perazzi, F.; Heilbron, F.C.; Wang, O.; Lin, Z.; Saenko, K.; Sclaroff, S. Real-time semantic segmentation with fast attention. *IEEE Robotics and Automation Letters* **2020**, *6*, 263-270.
- 54. Oršić, M.; Šegvić, S. Efficient semantic segmentation with pyramidal fusion. *Pattern Recognition* **2021**, 110, 107611.
- 55. Zhuang, J.; Yang, J.; Gu, L.; Dvornek, N. Shelfnet for fast semantic segmentation. In Proceedings of Proceedings of the IEEE/CVF International Conference on Computer Vision Workshops; pp. 0-0.
- 56. Poudel, R.P.; Liwicki, S.; Cipolla, R. Fast-scnn: fast semantic segmentation network. *arXiv preprint arXiv*:1902.04502 **2019**.
- 57. Yang, M.Y.; Kumaar, S; Lyu, Y.; Nex, F.; Real-time Semantic Segmentation with Context Aggregation Network. *ISPRS Journal of Photogrammetry and Remote Sensing* **2021**, *178*, 124-134.